Postprint of: Zima B., Wołoszyk K., Garbatov Y., Corrosion degradation monitoring of ship stiffened plates using guided wave phase velocity and constrained convex optimization method, OCEAN ENGINEERING Vol. 253 (2022), 111318, DOI: 10.1016/j.oceaneng.2022.111318

Corrosion degradation monitoring of ship stiffened plates using guided wave phase velocity and constrained convex optimisation method

Beata Zima[a], Krzysztof Woloszyk[a], Yordan Garbatov[b, 1]

[a] *Institute of Ocean Engineering and Ship Technology, Gdansk University of Technology, G. Narutowicza 11/12 st., 80-233 Gdansk, Poland*
[b] *Centre for Marine Technology and Ocean Engineering (CENTEC), Instituto Superior Técnico, Universidade de Lisboa, Avenida Rovisco Pais 1049-001 Lisboa, Portugal*

Abstract

The study presents an experimental investigation on the corrosion degradation level assessment using nondestructive wave-based methods. The degradation level of ship structural elements has been assessed in two different ways. The first one is based on the spectral decomposition and zero-crossing incorporated reconstruction of the dispersion curve approach of the antisymmetric Lamb wave mode and the best matching of the theoretical solution. The second approach was based on searching for a solution to the convex optimization problem. In the first case, the plate thickness is assumed to be constant and the phase velocity reconstructed curve is fitted to match the best solution in the all considered frequency domain. In the second case, the assumption about the varying plate thickness is set and the optimal thickness distribution resulting in any times of wave flight is defined.

Keywords:

corrosion degradation; steel plates; ship structures; non-destructive testing; guided waves

[1] Corresponding author e-mail: yordan.garbatov@tecnico.ulisboa.pt; Telf (351) 21 841 7907

1 Introduction

Ships and offshore structures operating in the marine environment are subjected to a severe corrosion environment (Melchers, 2008). The corrosion will primarily cause the reduction of the thickness of structural elements, which in consequence will lead to different structural failure modes (Saad-Eldeen et al., 2013; Woloszyk et al., 2018). One example is the sinkage of tanker Prestige ("Flashback history: Tanker Prestige sinking (Video)," 2015), where excessive corrosion degradation was found to be one of the main reasons for breaking the ship. Corrosion degradation was found to be one of the main reasons for breaking the ship. Therefore, in recent years significant attention has been paid to the development of corrosion detection and monitoring, e.g. employing electrochemical measurements (Xia et al., 2022).

There are typically two main types of corrosion, i.e. general and pitting one (Pedeferri, 2018) (see Figure 1). General corrosion is spread more within an entire element and causes rather non-uniform thickness reduction, where the level of non-uniformity depends on the corrosion medium and character. On contrary, pitting corrosion is a localized phenomenon and causes a significant reduction of the thickness in small regions of different sizes and shapes. In this view, these corrosion types should be treated separately in terms of diagnostics, evaluation and modelling.

Figure 1. The comparison between general (left) and pitting (right) corrosion (International Association of Classification Societies, 2015).

There are specified guidelines issued by Classification Societies, e.g. (International Association of Classification Societies, 2017), requiring to perform regular surveys during the service life of ships. Periodically, the thicknesses of structural elements are measured using an ultrasonic thickness gauge. This method has many advantages, e.g. is portable, user-friendly and reliable. However, apart from the advantages, several major disadvantages need to be pointed out. Firstly, the accuracy of this methodology is limited, especially when considering

corroded ageing structures (Cegla and Gajdacsi, 2016), since a smooth and clean surface is required to perform the measurement. Secondly, the measurements provide information about the resting thickness in one particular point only. It was found, that even for general corrosion, a significant variation of the plate thickness is observed (Guedes Soares et al., 2008; Woloszyk et al., 2021). Thus, to properly map the thickness distribution, numerous points need to be captured. For typical sizes of modern merchant ships (reaching the length of 400 m), capturing the detailed thickness distribution is rather impossible, especially taking into account the limited time of the survey. In this view, searching for other diagnostic methods seems to be essential.

With increasing awareness of the importance of maintaining the high quality and integrity of engineering structures by constant and thorough monitoring, the non-destructive evaluation (NDE) and structural health monitoring (SHM) methods attract more attention nowadays. The enormous contribution in the field of measurement devices (Astafev, 2019; Song et al., 2018), signal processing (Xia et al., 2016) and data analysis (Nash et al., 2018) is dedicated to corrosion detection and monitoring have been made. However, there is still a need to propose and develop new diagnostic methods. One of the very promising research areas is related to ultrasonic guided waves (GW). Their potential in the structural health assessment has been demonstrated in many previous studies devoted to diagnostics of metallic plates (Zima, 2021), pipes (Wu et al., 2022), composites (Fiborek and Kudela, 2021; Tschoke et al., 2021) or bolted joint connections (Ziaja and Nazarko, 2021).

Due to their capability to travel long distances without significant amplitude loss, guided waves seem to be useful in the diagnostics of large-scale objects like ship hulls. Their applicability would be an attractive alternative to standard inspection based on the ultrasonic thickness gauge which requires multiple measurements over a small area and does not provide sufficient information about the state of the whole structure. The possible application of guided waves in the corrosion degradation assessment has been demonstrated in many previous studies (Moustafa et al., 2014; Sharma and Mukherjee, 2010). The common assumption in the case of global corrosion says that the plate thickness changes uniformly. Because the thickness determines the solution of the dispersion equation, the resulting dispersion curves or wave velocity could be treated as an indicative parameter of the corrosion degradation progress (Farhidzadeh and Salamone, 2015).

The current study presents the modified approach of a corrosion degradation assessment of thin-walled plate structures. The corrosion degradation level is estimated based on the wave phase velocity determined by spectrum decomposition and the zero-crossing method of two adjacent signals captured at a known distance. Additionally, two different methods of

interpreting the results were proposed. In the first case, the assumption about the uniform thickness distribution of the corroded plate is adopted and the dispersion curve in the investigated frequency range is reconstructed to determine the current plate thickness. In the second approach, the assumption about uniform thickness distribution is not valid and the plate thickness is assumed to be irregular, but an assumption about the sparse representation of the vector describing plate thickness distribution is made. In consequence, the compressed sensing (CS) methods in corroded plate diagnostics are allowed. Additionally, the guided wave-based method for diagnostics of environmentally marine immersed corroded specimens is used for the first time which is an original contribution of the present study.

2 Ultrasonic assessment of corrosion degradation of thin-walled structures

This section describes the employed methodology. The algorithm in determining the plate thickness variability based on the convex optimization, which is the main original contribution of this study is preceded by the description of the procedure of the phase velocity determination and dispersion curve reconstruction presented already by other researchers (Draudviliene et al., 2021, 2018).

2.1 Wave phase velocity

Guided waves were extensively studied recently (Lamb, 1917; Mitra and Gopalakrishnan, 2016; Su et al., 2006). The classical problem of the Lamb wave propagation concerns the wave motion in an isotropic, homogeneous and elastic plate with uniformly distributed thickness. Two wave modes types can be distinguished depending on the wave patterns: symmetric and antisymmetric. Their velocity depends on excitation frequency and can be determined by solving the following equations:

$$\frac{\tan(qd)}{\tan(pd)} = -\frac{\left(k^2 - q^2\right)^2}{4k^2 pq}, \tag{1a}$$

$$\frac{\tan(qd)}{\tan(pd)} = -\frac{4k^2 pq}{\left(k^2 - q^2\right)^2} \tag{1b}$$

The parameters d and k indicate the plate thickness and wavenumber, respectively, while q and p are defined as:

$$p^2 = \frac{\omega^2}{c_L{}^2} - k^2, \quad q^2 = \frac{\omega^2}{c_T{}^2} - k^2.$$

where the longitudinal and transverse wave velocities c_L and c_T are dependent on the Lame's constants λ and μ and density ρ of the plate:

$$\begin{aligned} c_L &= \sqrt{\frac{\lambda + 2\mu}{\rho}} \\ c_T &= \sqrt{\frac{\mu}{\rho}} \end{aligned}, \tag{2}$$

Phase and group velocities, which are the solutions of Eq. (1) and usually are presented as dispersion curves, are defined as:

$$\begin{aligned} c_{ph} &= \frac{\omega}{k} \\ c_g &= \frac{d\omega}{dk} \end{aligned}. \tag{3}$$

The main idea of employing the guided waves in the corrosion degradation assessment is based on the assumption that corrosion degradation is related to changes in the plate thickness which involves changes in the dispersion curves. In the following study, the algorithm of corrosion degradation assessment based on phase the velocity curve reconstruction is presented. The guided wave propagation signals are processed using a combined method based on the spectrum decomposition and zero-crossing method (Mazeika et al., 2009). The main advantage of the proposed approach is that only two adjacent signals are essential in determining the curve segment and the distance between the transducers may be adjusted to the size of the tested specimen. So far, the wave phase velocity measurements were successfully conducted on undamaged metallic and composite plates (Draudviliene et al., 2021; Mazeika et al., 2009). Draudviliene et al. (2021) demonstrated a good agreement between numerical and experimental curves determined based on a hybrid approach. For clarity, the algorithm of the phase velocity determination as well as dispersion curve reconstruction is explained step by step in the following section, but it can be also found in (Draudviliene et al., 2021, 2018).

Two signals $s_1(t)$ and $s_2(t)$ registered at the distance *x* after applying the narrowband frequency excitation are processed and their frequency Fourier spectra $S(f)$ are determined. The next step involves the determination of the upper and lower limits f_L and f_H below and above which the spectra vanish, respectively. Within the frequency range (f_L, f_H) the spectra are filtered as:

$$\begin{aligned} U_{1,k}(f) &= S_1(f) B_k(f) \\ U_{2,k}(f) &= S_2(f) B_k(f) \end{aligned}, \tag{4}$$

where the *k*th filter is described by a Gaussian magnitude function:

$$B_k(f) = e^{4\ln(0.5)\left(\frac{f - f_L - (k-1)df}{\Delta B}\right)^2}, \tag{5}$$

In the following study, the parameter ΔB is determined as -6 dB bandwidth of the $S(f)$ which is associated with a power ratio of 0.25, k is the filter number while df is the frequency range of interest. The number of Gaussian filters n was adjusted to the spectrum bandwidth:

$$n > 1 + \frac{f_H - f_L}{\Delta B}, \tag{6}$$

Next, the inverse Fourier transform is used to synthesize the new signals from the filtered spectra:

$$\begin{aligned} S_{1,k}(t) &= \frac{1}{2\pi}\int_{-\infty}^{\infty} U_{1,k}(f) e^{i\omega t} d\omega \\ S_{2,k}(t) &= \frac{1}{2\pi}\int_{-\infty}^{\infty} U_{2,k}(f) e^{i\omega t} d\omega \end{aligned} \tag{7}$$

In consequence, two measured signals are decomposed into $2k$ components varying in the central frequency. To determine the phase velocity, corresponding to particular frequencies, the zero-crossing method is applied. For the established threshold T, the time of flight (ToF), the half period, and the frequency are determined (Figure 2):

$$c_{ph,k}^{i} = \frac{h}{t_{2,k}^{i} - t_{1,k}^{i}}, \tag{8}$$

$$f_k^i = \frac{1}{8}\left(\frac{1}{t_{1,k}^{i+1} - t_{1,k}^{i}} + \frac{1}{t_{1,k}^{i} - t_{1,k}^{i-1}} + \frac{1}{t_{2,k}^{i+1} - t_{2,k}^{i}} + \frac{1}{t_{2,k}^{i} - t_{2,k}^{i-1}}\right). \tag{9}$$

where h is the distance between the transducers. The set of the pairs $\left\{f_k^i, c_{ph,k}^i\right\}$ creates the dispersion curve representing the frequency-phase velocity relationship. The above procedure allows for reconstructing one segment of the dispersion curve. To determine the shape in a wider frequency range the measurement can be conducted for various excitation frequencies.

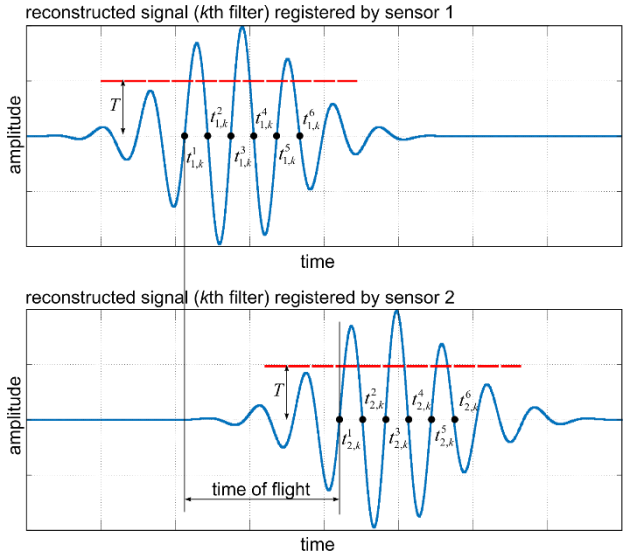

Figure 2 Time of flight, phase velocity and frequency based on zero-crossing approach

2.2 Degree of Degradation assessment based on dispersion curve fitting

The corrosion degradation level can be assessed by determining the plate thickness, which influences the shape of the dispersion curve. The main assumption of this approach concerns that corrosion degradation is uniformly distributed and thus, the thickness reduction is the same (uniform) within the analysed structure.

To determine the plate thickness, the dispersion curve as described by Eq. (1) and (3), is needed, which fits the best to experimentally determined curve and for this reason, the minimum mean squared error *Y* is the target:

$$Y(d) = \frac{1}{n}\sum_{i=1}^{n}\left(y_i(d)\right)^2 = \frac{1}{n}\sum_{i=1}^{n}\left(c_{ph}^{T,i}(d) - c_{ph}^{E,i}\right)^2, \tag{10}$$

were $c_{ph}^{T,i}(d)$ is the theoretically determined phase velocity for the thickness *d* obtained by solving the Lamb equations (Eq. (1)-(3)) and $c_{ph}^{E,i}$ is the experimental phase velocity.

2.3 Degree of Degradation assessment based on constrained convex optimization

In the second approach, the plate thickness is not assumed to be uniformly distributed. Thus, the wave velocity also varies along the propagation path as it depends on the plate thickness. To determine the average velocity along with the distance *h* the total time of flight *t* needed to travel from one sensor to another is calculated.

It is assumed that the plate of non-uniform thicknesses can be presented as an infinite number of finite elements in the form of a vector **x**, where each finite element of the plate corresponds to one particular thickness. The sum of the size of all finite elements in a line of

the vector **x** is equal to the distance *h* between sensors. To determine the ToF, essential to travel along with the finite element distances, each finite element size needs to be divided by the corresponding velocity calculated by solving the dispersion equation for considered finite element plate thickness. The sum of the times of flight will give the total ToF for the distance *h*. The following reasoning can be presented in the form of the equation:

$$\mathbf{V}_{1xn}\mathbf{x}_{nx1} = t\,, \tag{11}$$

where vector **V** represents the dictionary matrix containing the reciprocals of velocities. Because *t* depends on the frequency, the Eq. (11) can be reformulated and presented in a universal form:

$$\mathbf{V}_{mxn}\mathbf{x}_{nx1} = \mathbf{t}_{mx1}\,. \tag{12}$$

Now, the dictionary matrix **V** contains the reciprocals of the theoretical velocities and each column corresponds to a different thickness, while each row corresponds to a different frequency. As a result, the vector **t** contains the times of flight for finite frequencies. The dictionary matrix can be built using the theoretical analysis and dispersion solution or can be defined by experimental measurements. The times of flight are determined experimentally. The only unknown is the vector **x** containing the lengths of distances characterised by the same thickness. Solving the above equation is not straightforward because the matrix **V**, in general, is not square. In such a case the number of unknowns is greater than the number of equations (n>>m) and Eqn. (12) describes an underdetermined system of equations with an infinite number of possible solutions (infinite number of possible plates in which wave propagates with the same average velocity). The dictionary matrix may contain the information about the velocity for the infinite number of varying thicknesses but in real cases, the plate thickness may vary in a limited range (Figure 3). Thus, the vast majority of elements in the vector **x** will be 0. The assumption of sparse representation of the vector **x** allows for converting the underdetermined system of equations into an optimization problem:

$$\min \|\mathbf{x}\|_0 \quad s.t. \quad \mathbf{V}\mathbf{x} - \mathbf{t} = \mathbf{0}\,, \tag{13}$$

where the l^0 norm is the sum of non-zero elements of the vector **x**. The vector **x** is τ -sparsed if it contains τ non-zero elements. Unfortunately, because the vector $\|\mathbf{x}\|_0$ is nonconvex and discontinuous, this is an ill-posed inverse problem and solving the above equation is numerically unstable, NP-hard and its complexity increases exponentially with the number of unknowns.

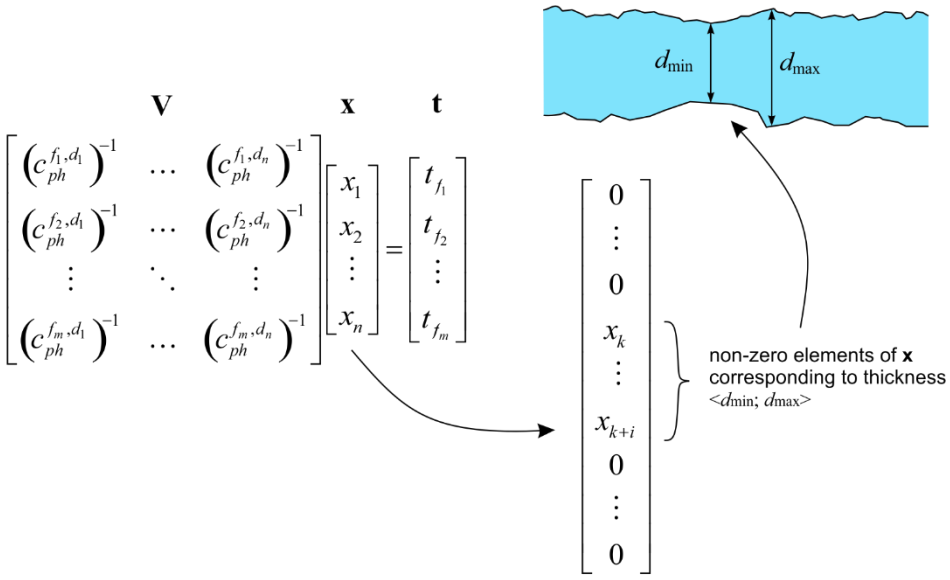

Figure 3 Graphical representation of the sparsity of vector x describing the plate thickness distribution

To avoid dealing with such problems, the l^0 norm can be substituted by the l^1 norm, which leads to the following form of the optimization problem:

$$\min \|\mathbf{x}\|_1 \quad s.t. \quad \mathbf{V}\mathbf{x}-\mathbf{t}=\mathbf{0}, \tag{14}$$

The global minimization of the l^1 norm, which is the sum of the absolute values of the vector $\mathbf{x}$ naturally leads to its sparse representation. An accurate reconstruction of the vector $\mathbf{x}$ can be accomplished by setting additional constraints.

First of all, in the considered case all elements of the vector $\mathbf{x}$ must be equal or greater than zero. Secondly, the sum of the distances must be equal to the distance between the transducers. Additionally, the experimental results might slightly differ from the theoretical predictions because of the additive noise, environmental effects, inaccuracies in ToF measurements, or material parameters. Taking into account the aforementioned constraints and the influence of inaccuracies ε bounded by $\|\varepsilon\| < \sigma$, the final form of the convex optimization problem can be written as:

$$\min \|\mathbf{x}\|_1 \quad s.t. \quad \begin{cases} \|\mathbf{V}\mathbf{x}-\mathbf{t}\|_2 \le \sigma \\ \sum_{i=1} x_i = h \\ \min\ \mathbf{x} \ge 0 \end{cases}, \tag{15}$$

The additional constraint may also concern the maximum finite element thicknesses of the corroded plate, which cannot be greater than the initial as-built thickness of the uncorroded stiffened plate.

The main difference between the methods based on phase velocity curve reconstruction and constrained convex optimization is the assumption about finite element thickness variability. In the first case, the plate thickness is uniform and can be described by one, average value. In the second case, any finite element of the plate is described by a different thickness which makes the corroded plate thickness nonuniformly distributed. The plate thickness variability can be described by a sparse vector in the thickness domain. The number of possible solutions resulting in the same ToF is considered to be infinite but because corrosion degradation in the vicinity is correlated, the sparse representation of the vector $\mathbf{x}$ is justified by the physical sense of such solution (Figure 3). The main advantage of both approaches is that only two signals registered in two different points on a tested stiffened plate with the known distance between sensors are required.

3 Experimental study

3.1 *Corrosion degradation*

The stiffened plates that are analysed here were subjected to accelerated marine immersed corrosion degradation. The corrosion test setup was described in detail in (Woloszyk et al., 2021). Thus, only the most important information is provided herein.

The corrosion testing aimed to provide conditions that simulate real seawater corrosion. Thus, the application of electric current was avoided and only natural factors were controlled to accelerate the corrosion degradation process. Particularly, the temperature was increased using a heating system, the water circulation was created using special pumps and oxygen content was increased by aeration. These conditions lead to the achievement of a corrosion rate reaching the level of 1 mm/year, which is much faster than typical conditions in operating ships (Soares et al., 2009), where the mean corrosion rate is closer to 0.1 mm/year.

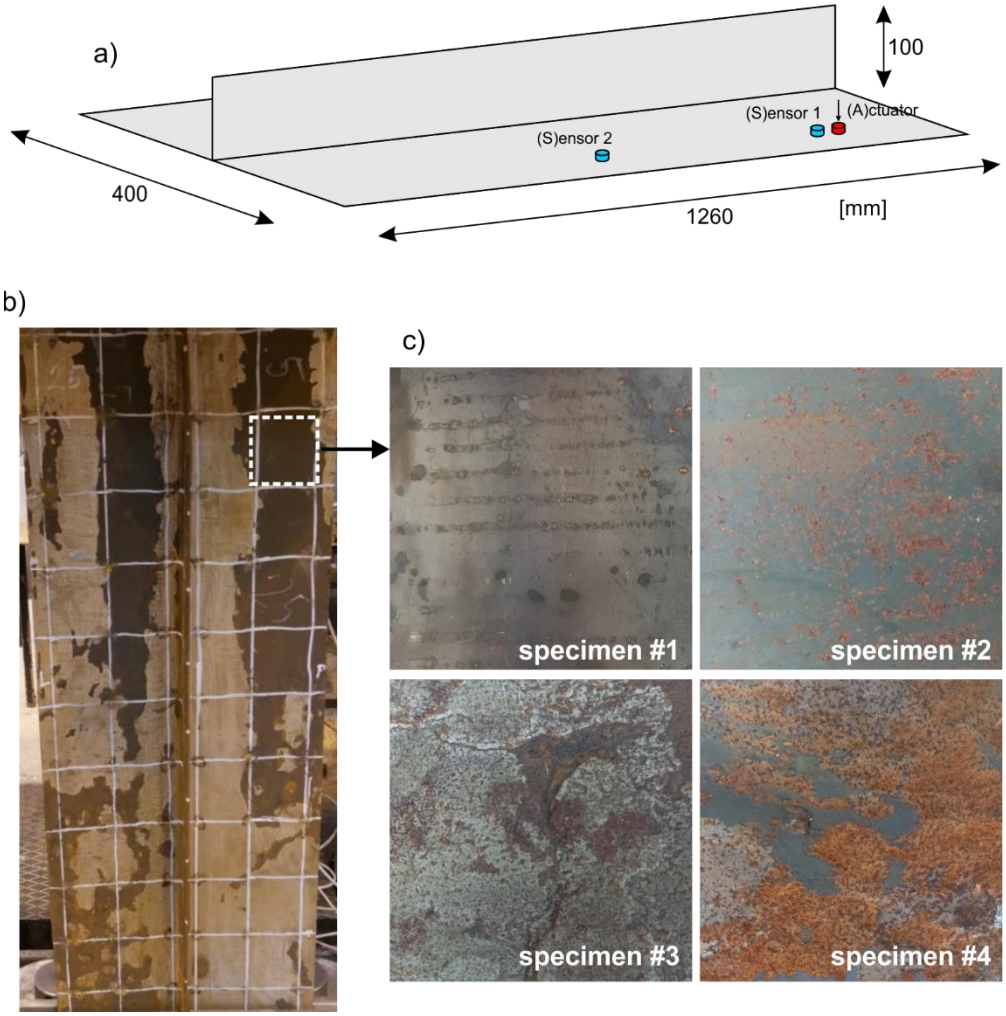

Figure 4. Experimental specimens: a) geometry, b) specimen #4, DoD=21% and c) corroded surfaces corroded surfaces (DoD=0%, 7%, 14% and 21%, respectively)

Different degradation levels measured as Degree of Degradation (DoD), which is estimated as the percentage loss of the mass were achieved. In particular, the DoD of 7%, 14% and 21% was achieved. In the present study, the stiffened plate specimens of an initial thickness of 5 mm were analysed. The geometry of all specimens, the example photo of the specimen of 21% of degradation level and zoomed surfaces of other specimens are shown in Figure 4. The material characterisation was performed during destructive tensile tests according to ISO standards (ISO, 2009). The elastic modulus was 198 GPa, Poisson's ratio v was 0.3 and the density ρ was 7,850 kg/m^3.

3.2 *Guided wave propagation*

The employed laboratory instruments comprised a function generator and oscilloscope amplified by a signal amplifier. The excitation function was applied in the form of a 5-cycle sine function modulated by a Hann window:

$$p(t) = \begin{cases} 0.5 p_0 \sin\left(2\pi ft\right)\left(1-\cos\left(\dfrac{2\pi ft}{n_w}\right)\right) & t \in \left[0, T_w\right] \\ 0 & t \geq T_w \end{cases}, \tag{16}$$

where f denotes the excitation frequency, p_0 is the excitation amplitude, T_w is the modulating window length and n_w is the number of time steps. The sampling frequency was 500 MHz, and the input voltage was 20 V. Each signal was averaged 1024 times to minimise the influence of the environmental effects. In the network, only three transducers were used: one for excitation and two for signal measurement. The distance h between the sensors attached by special wax on the plate surface was 30 cm (see Figure 4).

To find the most effective inspection frequencies in terms of a signal-to-noise ratio and wave mode content, the main study was preceded by the measurement of plate response under several excitation frequencies. The second aspect taken into account in the frequency selection was the wave sensitivity determined by the curve shape analysis. Figure 5 shows the set of phase velocity curves traced for plates varying in thickness. Because the compression type transducers attached to the plate surface were used in the experimental tests, the measurement concerns mainly the A0 Lamb wave mode which is associated with antisymmetric plane vibration. Therefore, the curves in Figure 5 were plotted only for this wave mode.

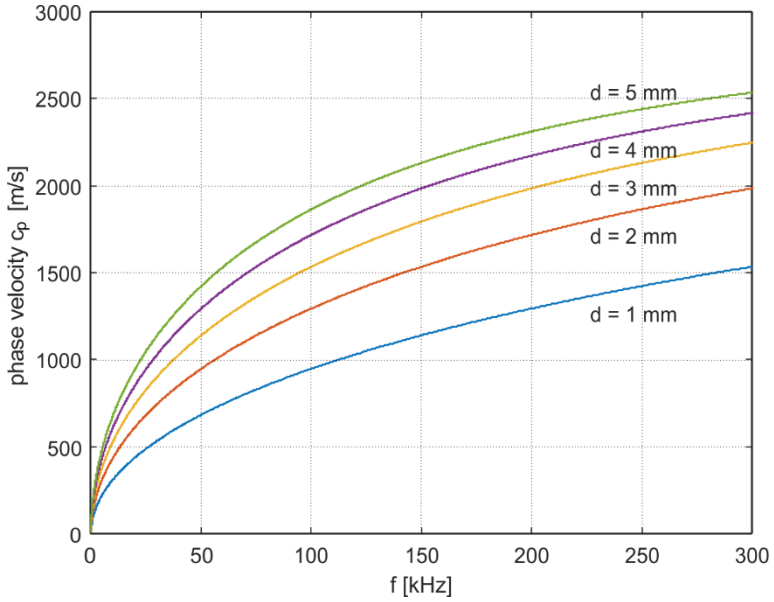

Figure 5 Phase velocity dispersion curves for steel plate (E=199 GPa, v=0.3, ρ=7850 kg/^{3}) varying in thickness

Based on the obtained results we can see that the A0 mode is highly dispersive in the low-frequency regime, which means that a small change in frequency results in a significant change in the velocity. For this reason, the accuracies between theoretical and experimental phase velocity obtained during the preliminary study were assessed as considerable and might be the source of the significant errors in curve reconstruction. Finally, the carrier frequencies used in the next step were from 150 to 250 kHz.

4 Analysis and results

4.1 *Tracing wave velocity dispersion curve*

Figure 6 shows the exemplary signals collected during the experimental campaign for specimens #1 and #4 for different excitation frequencies. The influence of the corrosion degradation is visible even at the early stage of the analysis. The character of the signals for corresponding frequencies differs significantly. In signals registered over specimen #1 (Figure 6a), three high-amplitude wave packets originated from wave interaction with the edges and stiffener are visible. The packets are easy to extract despite decreasing signal-to-noise ratio with increasing frequency. In the case of specimen #4 (Figure 6b), the shape of the incident wave is completely different. Its time duration is longer and it overlaps with low-amplitude reflections which were possibly triggered after interaction with surface irregularities. Thus, the extraction was much more difficult which in turn might affect the final results. The signals contain also a greater number of wave packets. Not only the reflections from boundaries and stiffener but also additional wave modes were registered, excited after mode conversion, which is a common phenomenon occurring in damaged structures. The sudden drop of the amplitude of the following reflections also unambiguously indicates the interaction with damage (Zima and Kędra, 2020). More intense wave dissipation and wave scattering caused by the corroded surface is manifested by faster wave damping.

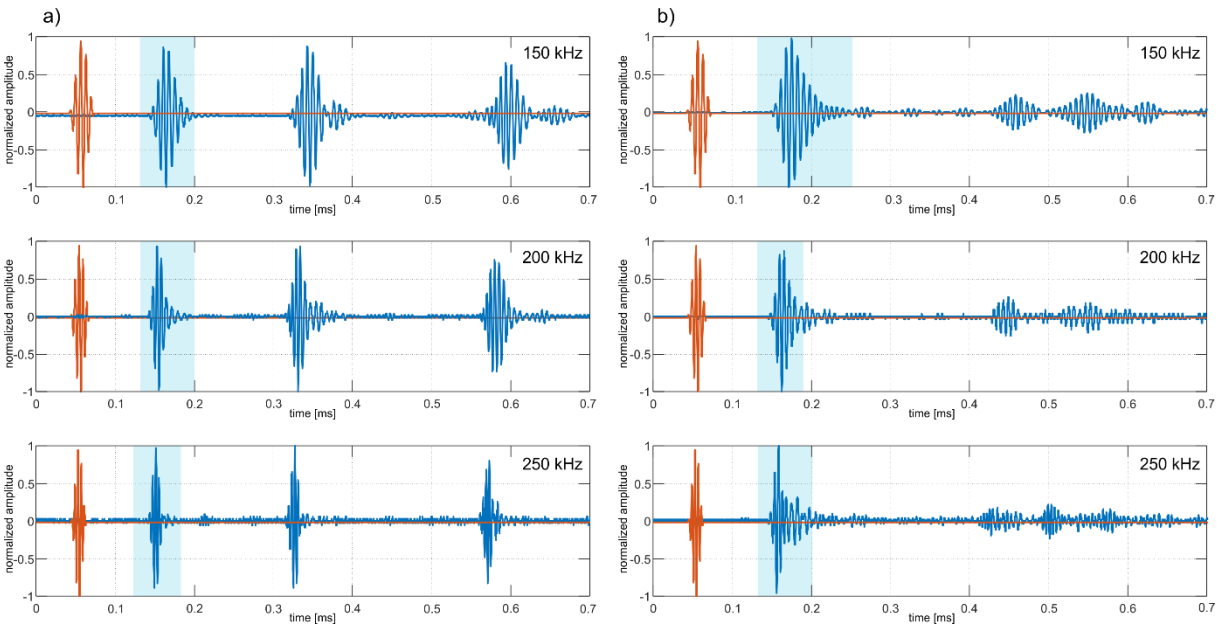

Figure 6 Experimental signals of wave propagation registered for a) specimen #1 and b) specimen #4. The input signals were plotted by the orange solid line, while output signals are plotted by the blue line

The indicated incident waves extracted from the signals were processed in the MATLAB environment according to the procedure described in Section 2.1. First, the wave phase velocity curve has been determined for an uncorroded specimen which allowed for estimation of inaccuracies of the proposed method and its further calibration. Because the majority of signal energy is concentrated around the maximum value of the amplitude, the threshold T was established as 0.9 to detect the zero-crossing time instances around the maximum amplitude and thus, minimise the influence of signal noise. The experimentally determined velocity is higher than theoretically predicted which stays in agreement with the results obtained by other studies (Mazeika et al., 2009). To avoid the inaccuracies in degradation level assessment caused by an overestimation of the phase velocity, in the first step the correction factor Δ was estimated. Its value was established by searching the minimum value of the following expression:

$$\sum_{i=1}^{n}\left((c_{ph}^{T,i}-\Delta)-c_{ph}^{E,i}\right)^2, \tag{17}$$

and was equal to 83 m/s. The same value of the coefficient was used to reduce the wave velocity obtained for other tested plates (Figure 7).

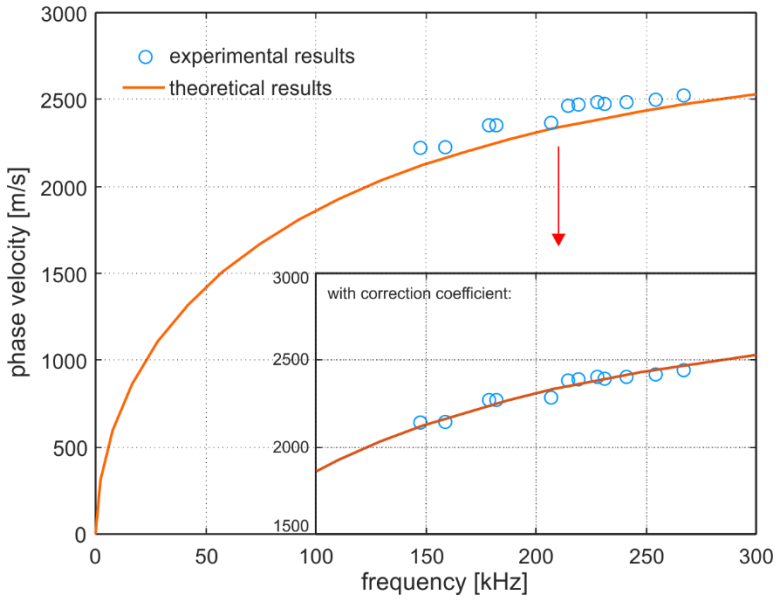

Figure 7 Theoretical and experimental phase velocity curve for uncorroded plate

The algorithm of the phase velocity determination has been used for tracing the curves for other thin-walled structures. The results in the form of experimental velocities and fitted curves are presented in Figure 8. It can be seen that the increase of the corrosion level degradation results in shifting the dispersion curve and decreasing the wave velocity associated with the certain spectral component. However, this effect is specific for the considered frequency range and utilised antisymmetric Lamb mode. In general, corrosion degradation may

cause an increase, decrease, or even may have no influence on wave velocity. Thus, it is crucial to choose the excitation parameters correctly.

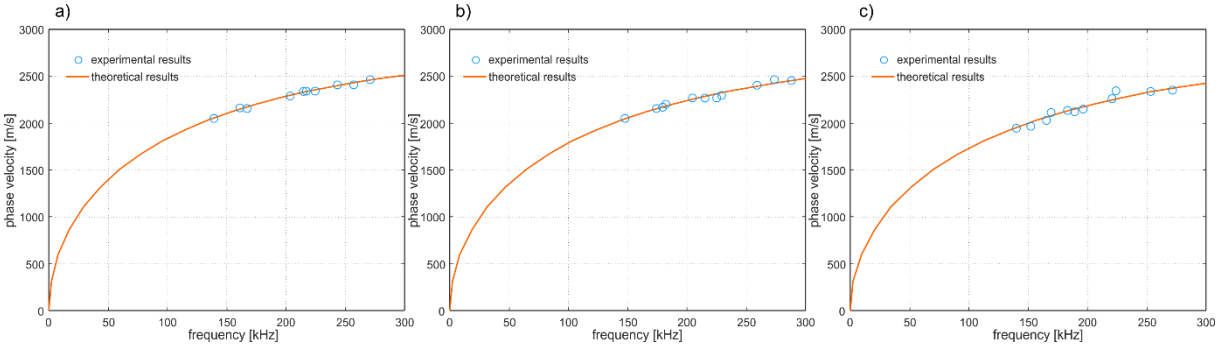

Figure 8 Theoretical and experimental phase velocity curve for corroded plate: a) specimen #2, b) specimen #3 and c) specimen #4

The average thickness *d* associated with reconstructed curves is equal to 4.820 mm, 4.475 mm and 4.105 mm, which corresponds to 3.6%, 10.5% and 17.9% of corrosion degradation level, respectively. In each case, the DoD is lower than obtained based on the weight measurement. However, the mass reduction was determined for the whole large-size specimen, while the velocity measurement was conducted at a certain distance along with the plate.

4.2 *Constrained convex optimization method in degradation level assessment*

Next, the problem of corrosion degradation level was considered assuming that the plate thickness is not uniformly distributed and it changes in a limited range. In the first step, the dictionary matrix has been built. In this study, the matrix contained reciprocals of theoretical velocities determined for experimentally obtained frequencies. The considered thickness range D_r for which the dictionary was built was 0 to 6 mm with a step of 0.001 mm. As mentioned above, the thickness of the corroded plate cannot be greater than the thickness of the uncorroded asbuilt plate (in this case 5 mm). On the other hand, the minimum thickness must be greater than zero. Otherwise, the wave would reflect from the gap and we would not have registered the signal that could be processed in the further stage. Therefore, the dictionary might be constructed for a narrower thickness range (i.e. 0.5 - 5 mm). However, because of the overestimation of wave velocity and inaccuracies in ToF measurement, the optimal solution of the convex problem may be found for the thickness out of the reasonable range.

The vector **t** was determined based on the results obtained from the curve reconstruction presented in Section 4.1. Vector **t** contains the ToFs calculated after the reduction of the phase

velocities. The value of σ, which was established using the dispersion curve for the uncorroded plate (Figure 7) was the same for all plates and it was 10^{-8}.

The constrained convex optimization problem was solved in the MATLAB environment (Grant and Boyd, 2008). The results of the analysis are presented in Figure 9. The graphs present the thickness variability of each plate. The horizontal axis indicates the thickness D_r, while the vertical axis denotes the length characterised by a certain thickness (vector **x**). According to compressed sensing theory, the majority of elements of the vector **x** are equal to 0.

In the case of uncorroded specimen #1 and specimen #2 with the lowest DoD, the function describing thickness distribution takes the form of single peaks. For specimen #1 two peaks were obtained: one for the thickness of 5.81 mm and one for 2.05 mm, which corresponds to a relatively insignificant distance (shorter than 1 cm). Moreover, between 2.05 mm to about 5.5 mm the values of **x** are equal to zero. Such thickness distribution suggests the step thickness change (from 5 mm to about 2) which in turn would be associated with additional reflections captured in signals. Because the signals measured for this specimen contained only incident waves (see Figure 6a), one can assume that the additional peak may result from an imperfect reconstruction of the dispersion curve. Based on the obtained results the average thickness has been calculated as the scalar product of vector **x** and vector D_r divided by the distance *h*:

$$d_a^{conv} = \frac{D_r \mathbf{x}}{h}, \tag{18}$$

The average thickness for the uncorroded was equal to 5.3 mm. It should be pointed out here that applying the additional constrain saying that the plate thickness cannot be greater than 5 mm would result in obtaining the peak value exactly for this thickness. On the one hand, it would be the perfect result, but on the other hand, it would be somehow forced by the reduction of the dictionary matrix size. Because it was the first attempt at using the compressed sensing methods in thickness estimation, the authors aimed to faithfully present also the drawbacks of the method. One of the drawbacks is the possible over or underestimation of the thickness because of the differences between the theoretical model and experimental measurements of wave propagation signals. The differences in actual and determined thicknesses are mostly the result of the ToF determination.

The possible solution for avoiding or reducing the unreasonable result is the calibration of the vector **t** based on the known thickness of the plate. In the current study, the velocity was calibrated based on the dispersion curve. However, it is also possible to calibrate the outcome vector **t**. The better approach would be also building the dictionary using the experimental results but it requires the measurements carried out on plates with various thicknesses. The

accuracy of the thickness distribution reconstruction would be dependent on the complexity of the dictionary.

The last factor influencing the results is the extent of the sensor network. The accuracy is greater for a more extensive network. However, it is crucial to find the trade-off between the number of sensors and measurements and the accuracy. In this study, the minimum required number of transducers is used, but the additional measurements, in different places or on different distances, may favourably influence the results.

In the case of specimen #2, three localised peaks were obtained (Figure 9b). The maximum thickness of 4.84 mm is considerably lower than in the previous case, which indicates the progress of corrosion degradation. Additional two peaks (3.459 mm and 4.815 mm) are also clearly visible. As previously, between the peaks no thickness variability was noted. The average thickness of specimen #2 was 4.71 mm.

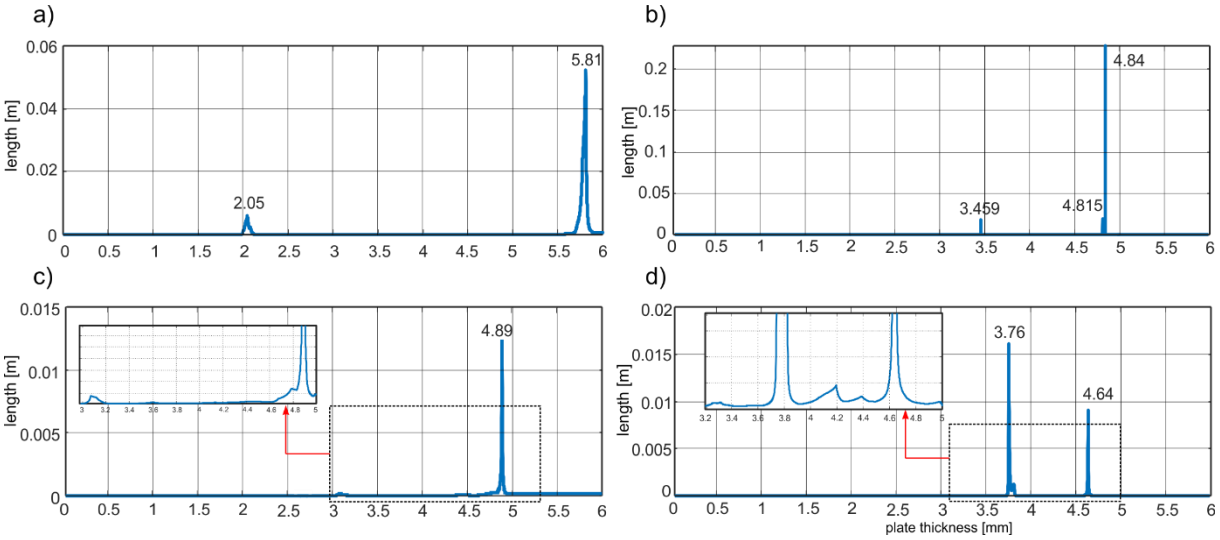

Figure 9 Plate thickness estimation by solving convex optimization problem for a) uncorroded plate, b) specimen#2, c) specimen#3, d) specimen#4

The maximum detected thickness for specimen #3 was 4.89 mm, which is higher than the thickness obtained for the less damaged specimen#2 (compare Figure 9b and c). However, this value was noted only on a very short distance of about 1.2 cm. Additionally, at the zoomed chart it can be seen several non-zero elements of the vector **x** corresponding to the thickness range from 3 mm to 5 mm. The results obtained for specimen#3 suggest that the plate thickness distribution is more complex this time. The average thickness of this specimen was 4.496 mm. Similar results were obtained for specimen#4 (Figure 9d). Despite three clear peaks for 3.76, 4.2 and 4.64 mm, the positive values of **x** were obtained for the other thicknesses. Thus, the average thickness of 3.994 mm is considerably lower than the maximum one.

4.3 *Discussion*

Figure 10 presents the results obtained by three different methods: by measuring the mass of the corroded specimen and calculation of the average thickness reduction, by reconstructing the phase velocity dispersion curves, and by solving the convex optimization problem. In each case the progress of damage degradation is visible. Despite differences between the main assumptions of the curve reconstruction method and convex optimization method the obtained averaged thicknesses are similar, which confirms the correctness of the conducted reasoning.

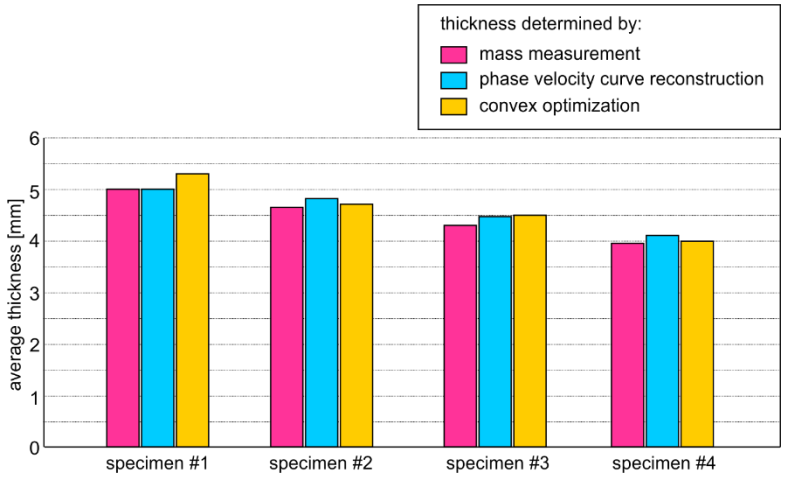

Figure 10 Comparison of average plate thickness determined using three different methods

In both cases, only two adjacent signals were essential to evaluate the DoD. The additional advantage of the convex-based method is that the state assessment of the tested element can be also made indirectly. The number of non-zero elements in vector **x** increases with the level of degradation. The corrosion degradation is associated with the occurrence of irregularities and thus, for a higher level of degradation, the plate thickness is described by a more complex function. Therefore, not only the average thickness can be treated as an indicator parameter, but also the complexity of the obtained solution.

The study demonstrated that the assumption about the uniformly distributed thickness reduction in the case of global corrosion is justified, but only in the case of low DoD. For specimens #1 and #2 (DoD equal to 0 and 7%), the functions representing thickness-distance relationships took the form of single localised peaks. In the case of higher DoD, the functions have very small but still non-zero values for intermediate thicknesses between the local maxima. Despite that, the most sparse vector **x** was searched in each case, a solution that would contain a smaller number of non-zero elements when satisfying the constraints of the total length and the positive value of each of the determined distances was not found.

The compressed sensing based on convex optimization can be potentially useful in assessing not only the global damage but also in estimating the thickness in the thinnest and the most corroded part of the specimen which is crucial for the correct prediction of the damage of the whole structure. However, for such assessment the holistic analysis of all obtained results is indispensable. In the considered case the minimal thickness was detected for uncorroded plate #1 but further analysis of the thickness distribution, as well as the signals which contained only incident waves, excluded the possibility of the existence of the step thickness change in the tested plate.

It should be mentioned here that the compressed sensing method used in the study is not suitable for the exact reconstruction of the plate thickness variability and therefore the results cannot be directly compared with exact thickness distribution determined e.g. by scanning the plate surface. The presented thickness distributions are the most sparse, optimal solutions of the convex problem which meet the additional requirements formulated in the form of constraints. However, the exact plate geometry can be defined by another thickness distribution for which the l^0 norm of vector **x** has higher values and thus was not an optimal one.

The proposed CS-based approach is the first attempt of taking into account the complex geometry of the corroded plate in the wave velocity estimation. The influence of the complexity of the geometry is visible in decreasing sparsity of the solution but the average thicknesses obtained using two different methods based on different assumptions do not vary considerably. The main reason for the small differences between averaged values is the relatively insignificant value of thickness deviation from the mean value. Despite the irregular surface, the corroded plates were almost uniformly damaged. The insignificant thickness change has in turn insignificant influence on the wave velocity, especially if it occurs at a very short distance. In Figure 11 the relationship between the phase velocity and plate thickness for various frequencies is depicted.

The thickness reduction from 5 mm to 4.5 mm causes a velocity decrease of about 50 m/s which is associated with increasing ToF. The ToF increase on the considered distance of 30 cm is equal to 0.002 ms. This value is comparable with the measurement accuracy. Moreover, for greater thicknesses (> 4 mm) the slope of the curve, which indicates the sensitivity of phase velocity to corrosion degradation and determines the effectiveness of its detection, becomes similar for all frequencies. It means that the change in velocity caused by thickness reduction is independent of the excitation frequency. Additionally, the curves become more “flat” which in turn means that the corrosion degradation becomes more difficult to detect and to evaluate in the case of thicker plates until only the first antisymmetric mode A0 is

incorporated into ultrasonic testing. The characteristics of the curves presented in Figure 11 explain why the greatest deviation in thickness assessment was obtained paradoxically for the uncorroded plate (see Figure 10).

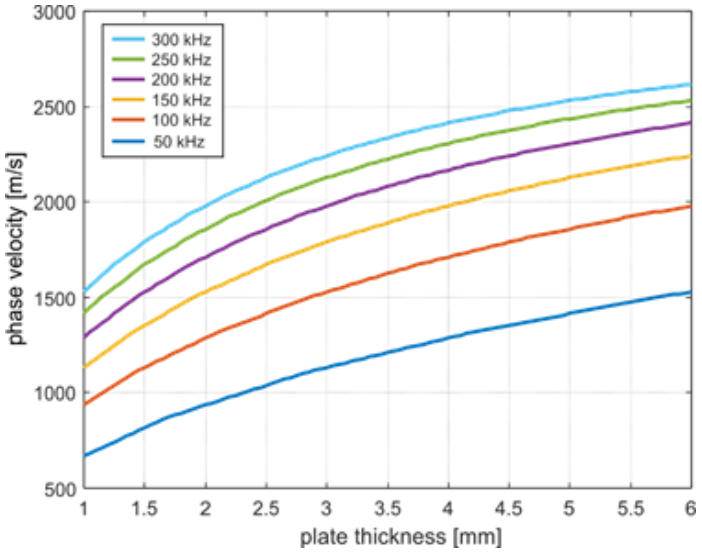

Figure 11 The relationship between the phase velocity and plate thickness for various frequencies

The presented study is the first step in the analysis of the inverse scattering problem aimed at the reconstruction of the exact thickness variability. However, such analysis must include the study of the frequency influence and waves interactions with irregularities. From wide literature about wave interaction with damages, it is known that damage detection requires employing wavelength comparable to damage size. If the damage occurs in the form of global corrosion with surface irregularities the wavelength should be comparable to the thickness deviation. For comparison, in the following study, the wavelength for 150 kHz was equal to 14.2 mm while for 250 kHz was equal to 9.9 mm. Significant length limits the possibility of the exact reconstruction of the plate geometry and thus, further investigation should include the high-frequency excitation. On the other hand, high-frequencies are associated with multimode propagation which can additionally convert after interaction with irregularities which extremely hinders the interpretation of the results, and therefore they were not incorporated at the early stage of the study.

5 Conclusions

To optimize the conventional ultrasonic thickness gauge measurement, this study proposes two wave-based methods for ship structural corrosion degradation monitoring. The effectiveness of the curve reconstruction and CS-based method has been verified experimentally on four large-scale corroded stiffened plates with a varying corrosion degradation level. The experimental results proved that both approaches can identify the thickness reduction. In the case of convex optimization, the progress of corrosion degradation could be also assessed based on the sparsity of the determined vector. The superiorities of the novel methods result from the minimal number of necessary measurements, limited sensor network and the possibility of monitoring the relatively large areas during a single measurement.

Acknowledgment

The first author greatly acknowledges the support of the Foundation for Polish Science (FNP). Partial financial support of these studies from the Gdańsk University of Technology by the DEC-04/2021/IDUB/II.1/AMERICUM ‘Excellence Initiative - Research University’program is gratefully acknowledged.

References

Astafev, E., 2019. The instrument for electrochemical noise measurement of chemical power sources. Rev. Sci. Instrum. 90, 025104. https://doi.org/10.1063/1.5079613

Cegla, F., Gajdacsi, A., 2016. Mitigating the effects of surface morphology changes during ultrasonic wall thickness monitoring, in: AIP Conference Proceedings. p. 170001. https://doi.org/10.1063/1.4940624

Draudviliene, L., Ait Aider, H., Tumsys, O., Mazeika, L., 2018. The Lamb waves phase velocity dispersion evaluation using a hybrid measurement technique. Compos. Struct. 184, 1156–1164. https://doi.org/10.1016/j.compstruct.2017.10.060

Draudviliene, L., Tumsys, O., Mazeika, L., Zukauskas, E., 2021. Estimation of the Lamb wave phase velocity dispersion curves using only two adjacent signals. Compos. Struct. 258, 113174. https://doi.org/10.1016/j.compstruct.2020.113174

Farhidzadeh, A., Salamone, S., 2015. Reference-free corrosion damage diagnosis in steel strands using guided ultrasonic waves. Ultrasonics 57, 198–208. https://doi.org/10.1016/j.ultras.2014.11.011

Fiborek, P., Kudela, P., 2021. Model-Assisted Guided-Wave-Based Approach for Disbond Detection and Size Estimation in Honeycomb Sandwich Composites. Sensors 21, 8183. https://doi.org/10.3390/s21248183

Flashback history: Tanker Prestige sinking (Video) [WWW Document], 2015. URL https://www.vesselfinder.com/news/4776-Flashback-history-Tanker-Prestige-sinking-Video (accessed 10.1.20).

Grant, M.C., Boyd, S.P., 2008. Graph Implementations for Nonsmooth Convex Programs (a tribute to M. Vidyasagar), in: Blondel, V., Boyd, S., Kimura, H. (Eds.), Recent Advances in Learning and Control. Springer London, London, pp. 95–110. https://doi.org/10.1007/978-1-84800-155-8_7

Guedes Soares, C., Garbatov, Y., Zayed, A., Wang, G., 2008. Corrosion wastage model for ship crude oil tanks. Corros. Sci. 50, 3095–3106. https://doi.org/10.1016/j.corsci.2008.08.035

International Association of Classification Societies, 2017. PR No 19. Procedural Requirement for Thickness Measurements.

International Association of Classification Societies, 2015. Recommendation 87. Guidelines for coating maintenance & repairs for ballast tanks and combined cargo/ballast tanks on oil tankers.

ISO, 2009. Metallic materials - Tensile testing - Part 1: Method of test at room temperature. Int. Stand. ISO 6892-1.

Lamb, H., 1917. On waves in an elastic plate. Proc. R. Soc. London. Ser. A, Contain. Pap. a Math. Phys. Character 93, 114–128. https://doi.org/10.1098/rspa.1917.0008

Mazeika, L., Draudviliene, L., Zukauskas, E., 2009. Influence of the dispersion on measurement of phase and group velocities of Lamb waves. Ultrasound 64, 18–21.

Melchers, R.E., 2008. Development of new applied models for steel corrosion in marine applications including shipping. Ships Offshore Struct. 3, 135–144. https://doi.org/10.1080/17445300701799851

Mitra, M., Gopalakrishnan, S., 2016. Guided wave-based structural health monitoring: A review. Smart Mater. Struct. 25, 053001. https://doi.org/10.1088/0964-1726/25/5/053001

Moustafa, A., Niri, E.D., Farhidzadeh, A., Salamone, S., 2014. Corrosion monitoring of post-tensioned concrete structures using fractal analysis of guided ultrasonic waves. Struct. Control Heal. Monit. 21, 438–448. https://doi.org/10.1002/stc.1586

Nash, W., Drummond, T., Birbilis, N., 2018. A review of deep learning in the study of materials degradation. Mater. Degrad. 2, 37. https://doi.org/10.1038/s41529-018-0058-x

Pedeferri, P., 2018. Corrosion Science and Engineering, Engineering Materials. Springer International Publishing, Cham. https://doi.org/10.1007/978-3-319-97625-9

Saad-Eldeen, S., Garbatov, Y., Guedes Soares, C., 2013. Ultimate strength assessment of corroded box girders. Ocean Eng. 58, 35–47. https://doi.org/10.1016/j.oceaneng.2012.09.019

Sharma, S., Mukherjee, A., 2010. Longitudinal Guided Waves for Monitoring Chloride Corrosion in Reinforcing Bars in Concrete. Struct. Heal. Monit. 9, 555–567. https://doi.org/10.1177/1475921710365415

Soares, C.G., Garbatov, Y., Zayed, A., Wang, G., 2009. Influence of environmental factors on corrosion of ship structures in marine atmosphere. Corros. Sci. https://doi.org/10.1016/j.corsci.2009.05.028

Song, S.-Z., Zhao, W.-X., Wang, J.-H., Li, J., Gao, Z.-M., Xia, D.-H., 2018. Field Corrosion Detection of Nuclear Materials using Electrochemical Noise Technique. Prot. Met. Phys. Chem. Surfaces 54, 340–346. https://doi.org/10.1134/S2070205118020211

Su, Z., Ye, L., Lu, Y., 2006. Guided Lamb waves for identification of damage in composite structures: A review. J. Sound Vib. 295, 753–780. https://doi.org/10.1016/j.jsv.2006.01.020

Tschoke, K., Mueller, I., Memmolo, V., Moix-Bonet, M., Moll, J., Lugovtsova, Y., Golub, M., Venkat, R.S., Schubert, L., 2021. Feasibility of Model-Assisted Probability of Detection Principles for Structural Health Monitoring Systems Based on Guided Waves for Fiber-

Reinforced Composites. IEEE Trans. Ultrason. Ferroelectr. Freq. Control 68, 3156–3173. https://doi.org/10.1109/TUFFC.2021.3084898

Woloszyk, K., Garbatov, Y., Kowalski, J., 2021. Indoor accelerated controlled corrosion degradation test of small- and large-scale specimens. Ocean Eng. 241, 110039. https://doi.org/10.1016/j.oceaneng.2021.110039

Woloszyk, K., Kahsin, M., Garbatov, Y., 2018. Numerical assessment of ultimate strength of severe corroded stiffened plates. Eng. Struct. 168, 346–354. https://doi.org/10.1016/j.engstruct.2018.04.085

Wu, J., Yang, F., Jing, L., Liu, Z., Lin, Y., Ma, H., 2022. Defect detection in pipes using Van der Pol systems based on ultrasonic guided wave. Int. J. Press. Vessel. Pip. 195, 104577. https://doi.org/10.1016/j.ijpvp.2021.104577

Xia, D.-H., Deng, C.-M., Macdonald, D., Jamali, S., Mills, D., Luo, J.-L., Strebl, M.G., Amiri, M., Jin, W., Song, S., Hu, W., 2022. Electrochemical measurements used for assessment of corrosion and protection of metallic materials in the field: A critical review. J. Mater. Sci. Technol. 112, 151–183. https://doi.org/10.1016/j.jmst.2021.11.004

Xia, D.-H., Song, S.-Z., Behnamian, Y., 2016. Detection of corrosion degradation using electrochemical noise (EN): review of signal processing methods for identifying corrosion forms. Corros. Eng. Sci. Technol. 1–18. https://doi.org/10.1179/1743278215Y.0000000057

Ziaja, D., Nazarko, P., 2021. SHM system for anomaly detection of bolted joints in engineering structures. Structures 33, 3877–3884. https://doi.org/10.1016/j.istruc.2021.06.086

Zima, B., 2021. Damage detection in plates based on Lamb wavefront shape reconstruction. Measurement 177, 109206. https://doi.org/10.1016/j.measurement.2021.109206

Zima, B., Kędra, R., 2020. Detection and size estimation of crack in plate based on guided wave propagation. Mech. Syst. Signal Process. 142, 106788. https://doi.org/10.1016/j.ymssp.2020.106788